Seismic Strengthening of Arches at Mount Khajeh Using FRP Rebars Under the Sarpol-e Zahab Earthquake in Iran

Shahraki M.[1*], Miri A.[2]

Abstract

Masonry arches stand out as some of the most valuable, significant, and defining components of traditional Iranian architecture. These structures have been admired throughout history for their aesthetic appeal and structural resilience, earning recognition as masterpieces of architecture and civil engineering both in Iran and globally. The Mount Khajeh archaeological site, which includes the ancient Mount Khajeh Palace and Kafro Castle from the Parthian-Sassanid era, is located in the Mount Khajeh rural district, Hamoun County, Sistan and Baluchistan Province. The arches at this historical site represent some of the most essential and treasured elements of traditional Iranian structural design. However, no prior research has been conducted to assess the seismic impacts on these arches or to propose methods for their retrofitting. This study aimed to address this gap by first developing a general model in ABAQUS to analyze the overall behavior of a representative arch. The most critical section of the arch was then isolated and modeled as a sub-representative of the entire structure. Using a simplified micro-level approach, both frictional and cohesive behaviors were incorporated at the block-mortar interfaces. Time-history dynamic analysis was performed on the selected arch using acceleration records from significant global earthquakes and one event recorded in Iran. These records were sourced from the Pacific Earthquake Engineering Research (PEER) Center's database. The findings reveal that, in terms of energy absorption, displacement, ductility, response modification factor, and maximum base shear, the first arch model demonstrates superior seismic resistance compared to two other arch models. Additionally, the results show that modeling and analyzing the arch in both its retrofitted and unstrengthen states significantly enhance its lateral load resistance, improve its seismic performance, and refine the crack distribution pattern. Furthermore, the application of the NSM-FRP strengthening technique minimizes damage and preserves the original appearance of the arch.

Keywords: Arch, Mount Khajeh, Retrofitting, FRP Rebar, Sarpol-e Zahab

✉*Corresponding author Email: Mehdishahraki2@gmail.com
1,2 Department of Civil Engineering, Zahedan Branch, Islamic Azad University, Zahedan, Iran

1. Introduction

These old structures, once called marvels, run the risk of being lost in the shadow cast by today's advances in technology. These older buildings, built without the aid of steel or concrete, are by no means less stable compared to today's reinforced or concrete-framed structures. Close observation of these heritage forms, aided by an engineer's eye trained in the present day, shows that they were none less than timely solutions for their time. Instead, they remain both relevant and adaptable in current practice [1]. From a structural point of view, the ideal arch is one that resists its loads by compressive action alone, without any tendency to bend upward or buckle. Since it is theoretically impossible to construct a purely compressive arch—because bending inevitably accompanies compressive forces—it is nevertheless possible to design arches in which compressive behavior predominates. Cracks appear in most historic buildings after some time due to aging, environmental exposure, and poor load transfer to the ground. These fissures multiply inside the structure and eventually cause the failure of the structure if not treated properly. Providing a continuous load path will help to reduce the crack appearance and further deterioration of the structure [2]. Earthen buildings, characterized for their large mass, low tensile strength, and brittle response of the material, have long been those that have usually demonstrated fatal vulnerability to damage. Their main failure patterns during seismic loadings start at the junction area between roof and wall since vertical cracking initiates quickly there [3]. In the last decades, the NSM technique has been widely developed and applied for structural strengthening. This strengthening method consists of embedding reinforcing bars of rectangular or round shape into shallow grooves opened near a member surface and then filling the groove opening with a compatible adhesive. The NSM approach improves the service-level behavior by reducing deflection, delaying crack initiation, and increasing the load at which cracks first appear, provided it is possible to create such surface grooves [4]. For instance, performed seismic stability analysis of some Iranian masonry arches. Several common types of arches were modeled in AutoCAD and then analyzed for gravity, live, and seismic loads using the finite element method in ANSYS. Static, free-vibration, linear, and nonlinear dynamic analyses were carried out using three different ground motion records. These values of given provided the evidence that the parabolic arches have performed better, carrying the load as compared to the other forms. Along with a time, the mode of collapse was determined and the initial crack. In another research paper, Amorhosein Karimi et al. (1397) investigated the cyclic behavior of classical Iranian arches. The different common types that were analyzed were six: Chille Chapar, Tokh-morgi or egg-shaped, and some pointed and elliptical geometries. This analysis has kept the material characteristics for Abaqus constant; they only changed the geometrical parameters for the arch. Besides, they did model representations of the arch and the walls at a macro level with material patterns that emulate concrete. The test results showed that the lateral load-carrying capacity of those arch types was relatively similar, and there was no significant difference among them[6].

In another study, Rahmatabadi, M. A. R. et al. (1396) have explained arch structure from a structural engineering philosophy. Of course, the analysis of moving load, type of force, and arch system sheds light on ways of development of arched thrust forces. Besides,

it can shed light onto the reasons how and why that an arch has stability even in all kinds ofstresses[7].

Batan and Kurnin, for their part, recently analyzed how six arches of different static schemes performed under the action of seismic vertical components. Using, subsequently, linear spectral and also linear and nonlinear time histories they gave some recommendations about which and how to take the vertical seismic effects into the load combinations in order for it to be possible to attain more appropriate and resistant structure designs [8].

In fact, an extended multi-hazard reliability analysis of a historic brick minaret subjected to wind and earthquake hazards was recently performed by Pouraminian et al. [9], which is located in Gaskar, Iran. Advanced finite element modeling, combined with the provision of national building codes, has been considered by the authors for appropriately capturing the structural behavior under the above-mentioned hazards. Monte Carlo simulations were amongst the probabilistic approaches used in evaluating the minaret structural safety for various loading cases by the authors. Their results indicated that whereas the structure performed satisfactorily under the design wind loads, it was notably vulnerable under seismic events.In the paper by Pinar Usta [10], seismic performance was analyzed by While these studies together contribute to the understanding of arch behavior, none of them have been specifically directed towards the capacity evaluation and retrofitting of the historical arches at Mount Khajeh. Thus, the present study seeks to investigate the stress distribution and tensile capacity of these very arches and to propose an appropriate strengthening method that would enhance the structural performance of the overall arches.

2. Theoretical Framework

using finite element modeling and fragility analysis of five historic masonry minarets in Antalya, Turkey. The results indicated that the geometric transitions, especially in transitional segments and balconies, develop concentrated stresses and potential failure zones. In order to enhance the structural resistance against lateral forces such as earthquakes and wind, smoother transitions and tension rings were recommended. This research study hereby underlines the need for selective strengthening and retrofitting strategies, especially for the preservation of architecturally valuable monuments located in seismically active regions. Besides, material property uncertainties together with the limited feasibility of performing destructive tests make historic masonry arch bridges very susceptible to seismic loading. In this paper, Tornado diagrams and finite element modeling via ANSYS were used to analyze the sensitivity of structural responses in a representative case study of an arch bridge. The main conclusion derived is that the backfill elasticity modulus and infill material density are some of the most critical factors that govern stress distributions and displacements. These results emphasize the importance of considering material property uncertainties in seismic vulnerability assessments of historic arch bridges [11].

2.1. About Mount Khajeh

Mount Khajeh, also known as Mount Oshida and Mount Rostam, is located in Sistan Plain, 30 kilometers southwest of Zabol, Sistan and Baluchestan, Iran. Oshida is a Middle Persian word meaning “eternal.” Sacred in Islam, Christianity and Zoroastrianism, the trapezoid-shaped mountain is made up of black basalt and stands at 609 meters above sea level in the middle of Hamun Lake. The Mount Khajeh archaeological site is a unique

fortress from the Parthian and Sassanid periods. Commonly referred to as the "adobe Persepolis," the colossal structure is the only surviving Parthian fortress in Iran. A large number of artifacts from the Sassanid and Parthian periods as well as remains of Muslim and Buddhist places of worship have been discovered on the site [12]. Figure 1 depicts the geographical location of Kuh-e Khwāh, as well as a view of the fortress and arches situated on the mountain.

Figure 1. The geographical location of Kuh-e Khajeh and a view of the fortress and arches located there.

The dimensions of the modeled arches, along with nomenclature used for its finite element modeling, is given in Tables 1 and 2. Material properties for materials used in arches and FRP rebars are listed in Tables 3 and 4.

Table 1. Dimensions of the Modeled Arches

Arch Model	Length (mm)	Width (mm)	Height (mm)
QS-1	5000	4000	3400
QS-2	500	4100	4250
QS-3	1500	3500	3000

Table 2. Nomenclature of Arches for Modeling

Arch type 1 (QS-1)	Unreinforced
Arch type 1 (QD-1)	Reinforced
Arch type 2 (QS-2)	Unreinforced
Arch type 2 (QD-2)	Reinforced
Arch type 3 (QS-3)	Unreinforced
Arch type 3 (QD-3)	Reinforced

Table 3. Mechanical Properties of the Adobe and Clay Materials Found in the Investigated Arches [12]

Shear strength (MPa)	Tensile strength (MPa)	Compressive strength (MPa)	Elastic modulus (MPa)
1.8	1.7	3.6	2000

Table 4. Properties of the FRP rebars [13]

Property	FRP rebar
Specific weight (MPa)	7.1
Ultimate stress (MPa)	701
Yield stress (MPa)	483
Compressive strength (MPa)	310-482
Tensile modulus (GPa)	55
Coefficient of thermal expansion	9.9

2.2. Earthquake data analysis

An accelerogram of an earthquake in Iran was used for dynamic time-history analysis of the arches. The accelerogram was drawn from the Pacific Earthquake Engineering Research Center (PEER) database and represents the Sarpol-e Zahab earthquake (Fig. 2). Tables 5 and 6 present the accelerogram specification.

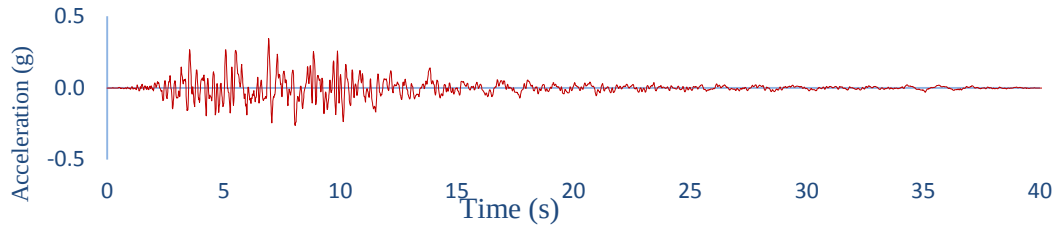

Fig. 2. The Horizontal Component of the Sarpol-e Zahab Earthquake Record

Table 5. Specifications of the Utilized Acceleration Record (PEER)

Accelerogram	Maximum acceleration (g)	Maximum speed (cm/s)	Maximum displacement (cm)	RSN
Sarpol-e Zahab	0.432	45.677	9.043	7384-1

Table 6. Sarpol-e Zahab earthquake specification

Magnitude	7.3
Date and time (local time)	21:48:16 2017-11-12
Longitude	45.9
Latitude	34.84
Depth	11 (km)

3. Methodology

3.1. Numerical Study

A comparison provided by Morshedi et al. [13] was reviewed to study the effect of reinforcement on adobe arch bridges, where they examined an arch-containing stone structure at a 1:1 scale under simultaneous vertical and lateral loads using Abaqus 2020 (Fig. 3). They applied the vertical and then the lateral load to the impost through a spring and the arch, respectively. In the first test, the sample was loaded without rebars, and the second sample was loaded after being reinforced with CFRP. The results indicate that the first cracks in sample 1 appeared in areas subjected to tensile force, leading to the use of CFRP for reinforcement in these vulnerable regions. The reinforced structure showed great strength against lateral forces. Furthermore, an equal elastic modulus of 4050 MPa was used to generate an elastic

response representing the real composition of the masonry (blocks and mortar). C3D8R elements were used systematically for meshing [14].

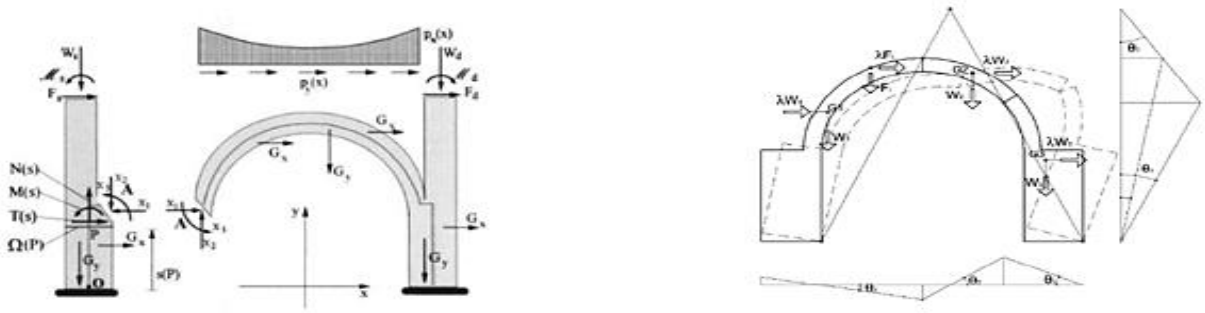

Fig. 3. Arrangements of lateral and radial anchorages in the studied bridge[13]

Figure 4 shows a numerical representation of the stresses appearing in the model. As Figures 5 and 6 show, there was an adequate overlap between the answers of our study and those of the aforementioned paper in modeling the vault of the *Asbad* windmill, validating the latter study's findings [15]

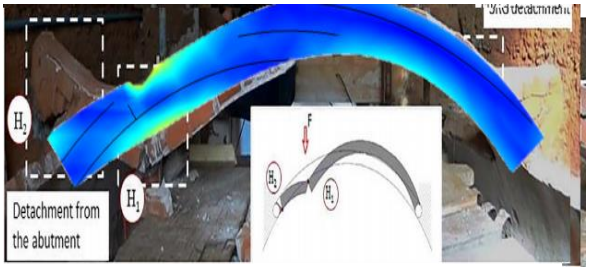

Fig. 4. Stresses in the mode

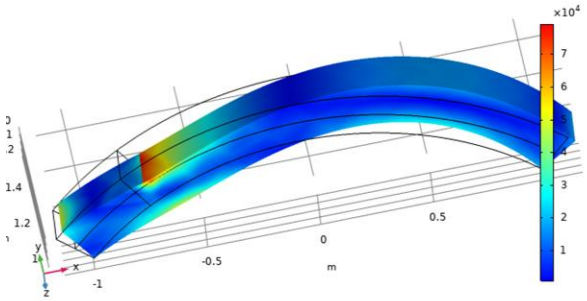

Fig. 5. Arrangement of the curve results for validation

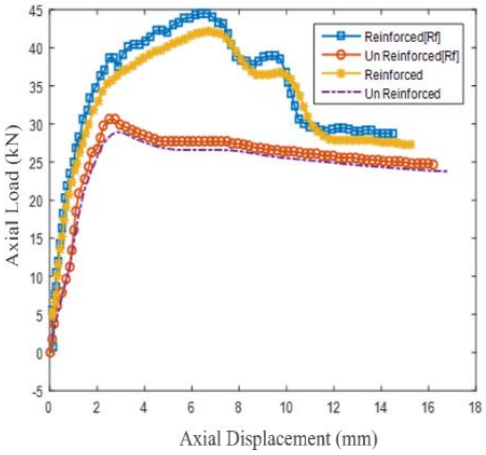

Fig. 6. Comparison of the force–displacement curve of the reference specimen with that of the validation specimen

3.2 Mesh Size Sensitivity Analysis

In this work, the mesh independence analysis has been performed for the geometry with the highest arch density to ensure that the results would also be valid for the other configurations. This geometry has been chosen because, given its high arch density, it produces the greatest resistance; therefore, establishing mesh independence for this case ensures its applicability in all other cases. Figure 7 shows how the resistance is changing on the arch resulting from five different meshings.

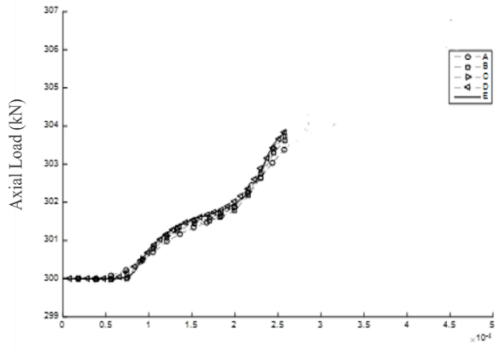

Fig.7. Variations in Strength Across Five Different Mesh Configurations

The steps in creating the mesh in the modeling process as applied, can be seen from Figure 8. The nodes for each of the five configurations are indicated in Table 7, together with error percentage and it can be seen that for configuration D, mesh

independency with less than 0.003 percent error was achieved.

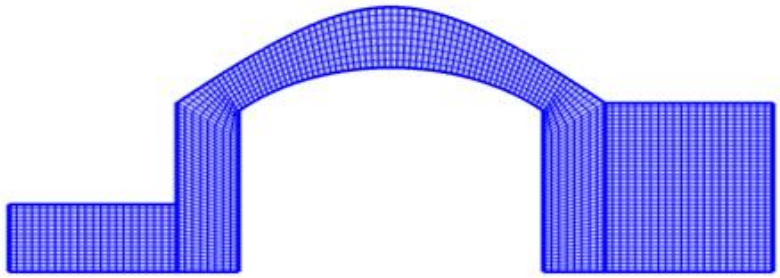

Fig.8. The steps in creating the mesh in the modeling process

Table 7. Number of Nodes and Error Percentage

Mesh	Number of Points	Error Percentage
Mesh A	5000	6.13
Mesh B	10000	4.11
Mesh C	25000	2.37
Mesh D	45000	0.0035
Mesh E	80000	0.0001

4. Result and Discussion

To conduct a nonlinear time-history dynamic analysis in Sarpol-e Zahab, the stress-strain curve of the materials was entered, and finally, using the base shear force-displacement curve, seismic parameters were derived. Keep in mind that there are two ways to place reinforcement bars used for strengthening: the first method uses the bars parallel with the crack path, while the second places them vertical to the crack path. Both methods are possible, but if the structure does not have existing cracks at the time of placement, they are better off placing

reinforcement bars perpendicularly to the line of anticipated cracking. Such an approach leads to better resistance because of the higher shear strength. But the downside of this approach is that it greatly affects the appearance of the structure.

Longitudinal bars were used as reinforcement only since no transverse reinforcement is needed with no longitudinal cracking. Thus, longitudinal bars were used to avoid high shear stress. Longitudinal bars with 13 cm spacing were used instead of transverse reinforcement to maximize shear strength without compromising structural integrity.

4.1. Analyzing the Group 1 models under the Sarpol-e Zahab earthquake

4.1.1. Results from QS1 Arch Modeling

Figure 9 shows an example of the Mount Khajeh arches along with the meshed example. The details were reproduced as accurately as possible.

Fig. 9. Arch model QS-1

Figure 10 illustrates that arch QS-1 exhibits good ductility. Additionally, Table 8 indicates that the behavior coefficient is favorable, considering the arch was constructed from Adobe.

Table 8. The results obtained from modeling the QS-1 arch under the Sarpol-e Zahab earthquake

Model	Ductility	Final Displacement	Energy absorption	Behavior coefficient
QS-1	3.3	0.12	8.2×10^6	2.32

As presented in Table 8 of the article, the QS-1 model demonstrates a ductility value of 3.3. Ductility, defined as the ratio of ultimate displacement to yield displacement, reflects the structure's capacity to endure significant plastic deformations beyond the yield point without experiencing a substantial reduction in strength. For this particular model, the

ultimate displacement was recorded at 12 cm, while the yield displacement was calculated to be 3.63 cm. These figures were derived from nonlinear time-history analyses and further validated by examining the base shear-displacement curve, as illustrated in Figure 37. The remarkable ductility exhibited by the QS-1 model is primarily attributed to the specific material properties employed and the optimized geometric design of the arch. These characteristics greatly improve the structure's ability to dissipate seismic energy effectively, thereby reducing the likelihood of sudden failure under dynamic loads.

The analysis of yielding and non-linear behavior in the arch components indicates that, in the model, yielding starts in the middle of the arch but, as shown in Figure 10, gradually progresses toward the bottom. Figure 11 shows the strain in model QS-1. Most of the strain, as is shown, is in the column bases, and there is a possibility of cracking in the arch. Figure 12 shows the maximum Displacement to be 12 centimeters. As expected, most of the Displacement t has occurred in the crown due to the thinness of masonry in that area.

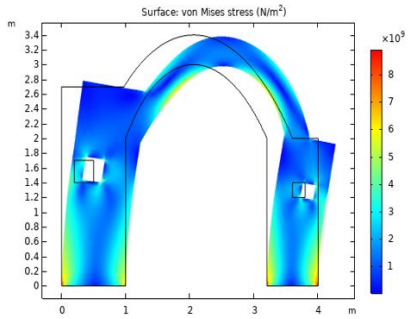

Fig. 10. Start of yielding in QS-1

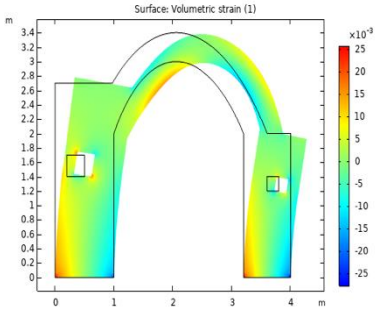

Fig. 11. Strain in QS-1

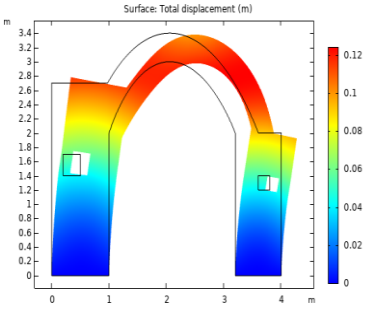

Fig. 12. Displacement in QS-1

4.1.2. Results from QS2 Arch Modeling

Figure 13 shows the arch QS-2 model. We tried to reproduce the details as accurately as possible.

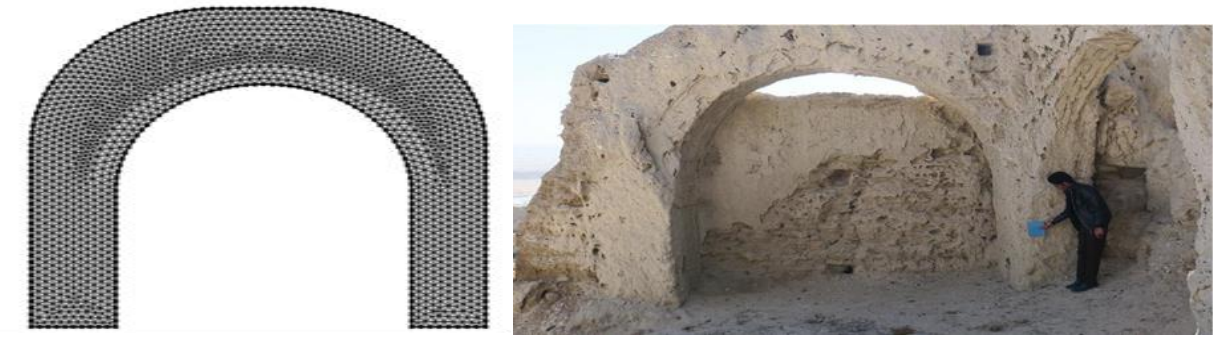

Fig. 13. Arch model QS-2

As shown in Table 9, QS-2 has good ductility, and the behavior coefficient has dropped by 3% due to the heavier load of the structure.

Table 9. The results obtained from modeling the QS-2 arch under the Sarpol-e Zahab earthquake

Model	Ductility	Final Displacement	Energy absorption	Behavior coefficient
QS-2	2.92	0.24	6.05×10^6	2.12

The analysis of the yielding and the non-linear behavior of the arch components shows that, in the unreinforced QS-2 model, yielding starts in the sides of the arch but, as shown in Figure 14, gradually extends toward the middle. Figure 14 shows the start of yield in QS-2. The yield stress has drastically increased, indicating that the structure is about to collapse. And as shown in Figure 15, the structure is subject to too much Displacement and has become hyperplastic. Figure 16 shows the maximum Displacement in QS-2. Stress is high and moving in the model, moving the structure as much as 200 millimeters.

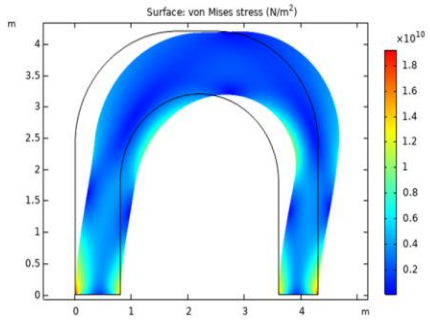

Fig. 14. Start of yielding in QS-2

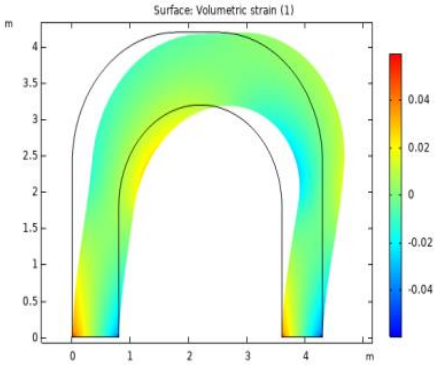

Fig. 15. Strain in QS-2

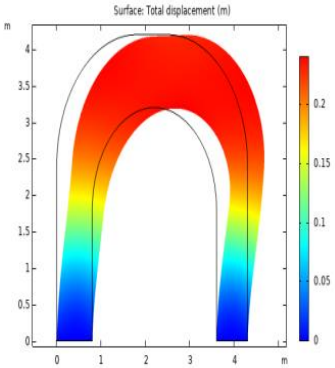

Fig. 16. Displacement in QS-2

4.1.3. Results from QS3 Arch Modeling

Figure 17 shows the QS-3 arch model developed in the Abaqus finite element software on the left and the actual arch specimen being investigated on the right at Kuh-e Khwaja.

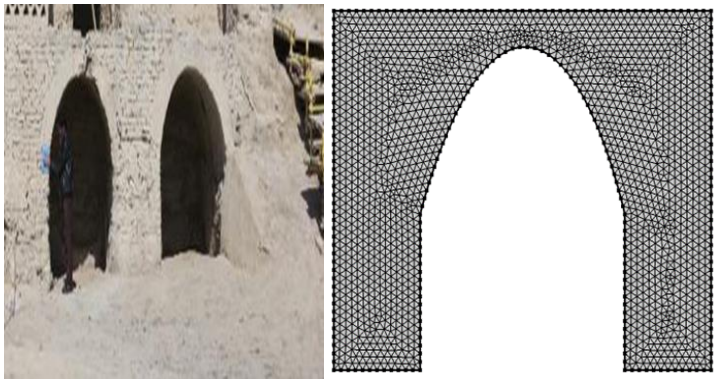

Fig. 17. Arch model QS-3

The information in Table 10 the ductility and response modification factor, which plays an important role in addressing the susceptibility of the structure under the studied seismic condition.

Table 10. The results obtained from modeling the QS-3 arch under the Sarpol-e Zahab earthquake

Model	Ductility	Final Displacement	Energy absorption	Behavior coefficient
QS-3	2.7	0.23	5.41×10^6	1.7

The analysis of the yielding's initiation and the nonlinear behavior's emergence in the arch components indicates that the yielding area grows from the edges in the QS-3 model of the unreinforced arch. As illustrated in Figure 18, the yielding spreads progressively to the neighboring arches. Figure 18. First instants of yielding in the QS-3 model. In this case, there is a 10% increase in stress levels, meaning the risk for arch failure is greatly increased. The strains along the QS-3 model are shown in Figure 19, while the displacements corresponding to the same model are presented in Figure 20. As expected, this arch also has the potential for failure. In addition, the values of the

displacement and plastic strain are larger than the two arch models mentioned above

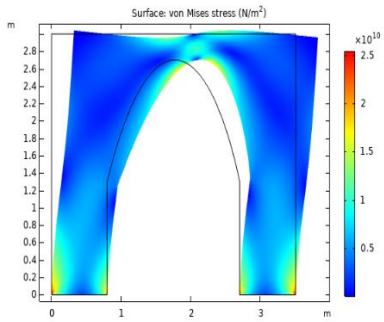

Fig. 18. Start of yielding in QS-3

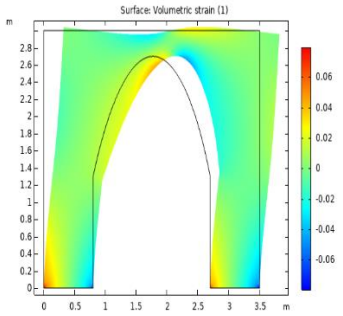

Fig. 19. Strain in QS-3

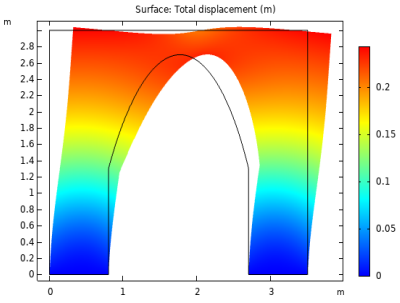

Fig. 20. Displacement in QS-3

4.2. Analyzing the Group 2 models under the Sarpol-e Zahab earthquake

4.2.1. Results from QD1 Arch Modeling

As Table 11 shows, based on the movement and the resulting base shear force, the reinforced QD-1 arch has greater ductility than its unreinforced counterpart

Table 11. The results obtained from modeling the QD-1 arch under the Sarpol-e Zahab earthquake

Model	Ductility	Final Displacement	Energy absorption	Behavior coefficient
QD-1	3	0.07	7.30×10^6	2.45

The analysis of the yielding and the non-linear behavior of the arch components indicates that, in the reinforced QD-1 model, yielding starts in and gradually expands throughout the wall. Figure 21 shows the start of yielding in QD-1. As expected, stress is highest in the columns. Figure 22 shows that the strain in QD-1 has increased by 15% compared to the unreinforced model. Figure 23 shows the displacement in QD-1, which is only slightly different than that of the other model.

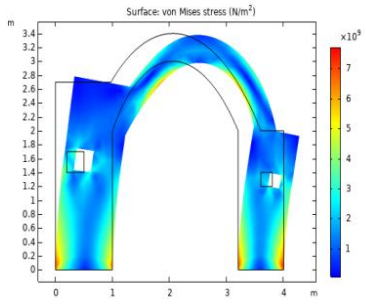

Fig. 21. Start of yielding in QD-1

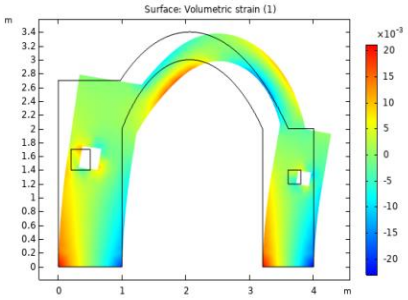

Fig. 22. Strain in QD-1

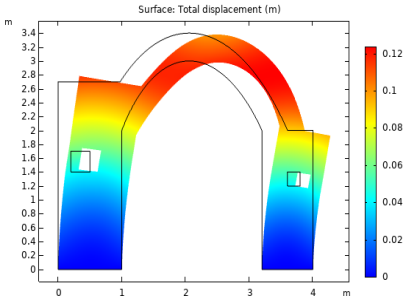

Fig. 23. Displacement in QD-1

4.2.2. Results from QD2 Arch Modeling

The yielding and non-linear behavior of the arch components (Fig. 24) shows that in the reinforced QD-2 model, yielding initiates inside and propagates through the wall. The strain in QD-2 is shown in Figure 25, and thedisplacement of the model is presented in Figure 26. We can see from Table 12 that the ductility of the reinforced QD-2 arch can be obtained by comparing the displacement and the base shear force generated. Moreover, the behavior factor of this model from the limit state design is significantly greater than that of the other model.

Table 12. The results obtained from modeling the QD-2 arch under the Sarpol-e Zahab earthquake

Model	Ductility	Final Displacement	Energy absorption	Behavior coefficient
QD-2	2.49	0.22	5.01×10^6	1.8

Table 13. The results obtained from modeling the QD-3 arch under the Sarpol-e Zahab earthquake

Model	Ductility	Final Displacement	Energy absorption	Behavior coefficient
QD-2	2.81	2.81	6.05×10^6	2.2

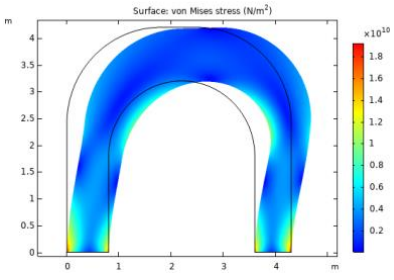

Fig. 24. Start of yielding in QD-2

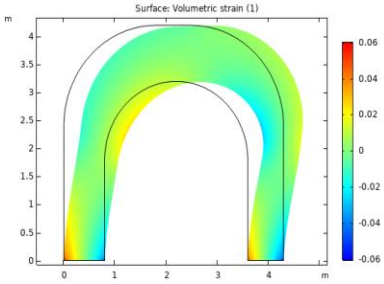

Fig. 25. Strain in QD-2

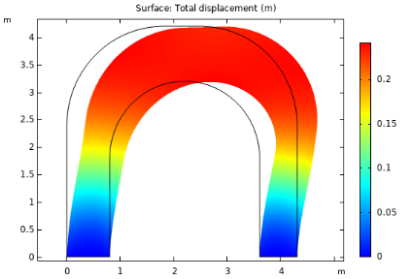

Fig. 26. Displacement in QD-2

4.2.3. Results from QD3 Arch Modeling

Table 13 presents the outcomes of the retrofitting applied to the targeted arch under the Sarpol-e Zahab earthquake. It is evident that ductility improves significantly in the retrofitted model compared to its non-retrofitted counterpart. Additionally, the behavior factor calculated through the limit states method is notably higher in the retrofitted model than in the model without retrofitting.

Figure 27 highlights the onset of yielding zones and the nonlinear response of the arch components. In the retrofitted QD-3 arch model, the yielding zones originate within the wall and progressively spread throughout it. Furthermore, Figure 28 illustrates the strain distribution in the QD-3 model, while Figure 29 depicts the displacement experienced under the earthquake load in the same model.

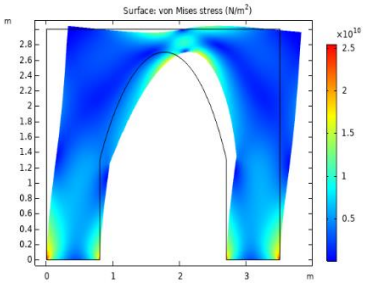

Fig. 27. Start of yielding in QD-3

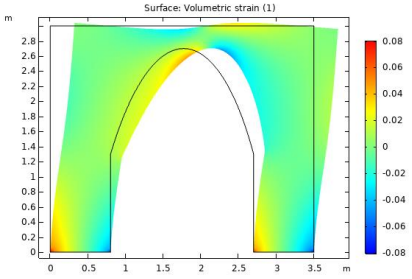

Fig. 28. Strain in QD-3

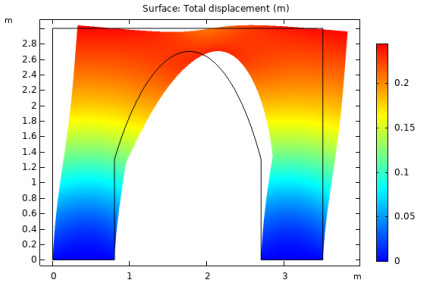

Fig. 29. Displacement in QD-3

4.3. Results for the QS-1 arch model under the Sarpol-e Zahab earthquake

Figure 30 shows the cracking pattern in the unreinforced QS-1. Areas with extensive cracking appear red and are prone to collapsing. Figure 31 shows a real-world example of the crack .

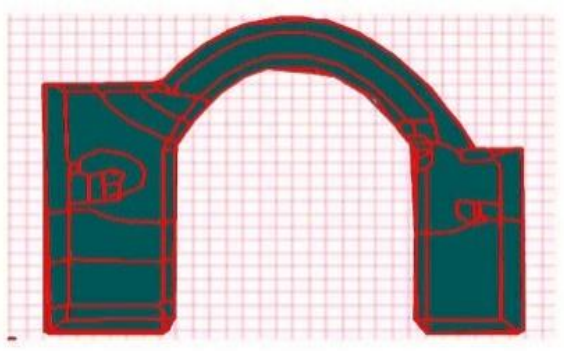

Fig. 30. Cracking pattern in QS-1

Fig. 31. Real-world example of the crack

After determining the cracking pattern (Fig. 32), we looked for the right place to carry out the NSM technique. To do so, we ran a MATLAB script as instructed on Mastork.com, established the depth of the crack (Fig. 33), nd placed the rebars as instructed by Sakbana et al. [16] (Fig. 33). Figure 34 shows the resulting mesh. As can be seen, the mesh is more concentrated in the reinforced area.

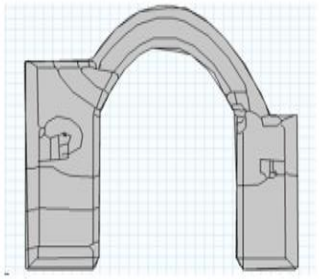

Fig. 32. Cracking pattern in QS-1

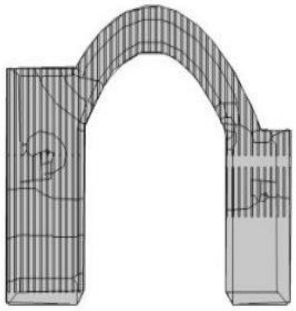

Fig. 33. Rebar placement in QS-1

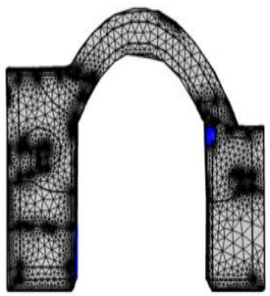

Fig. 34. Resulting mesh after rebar placement in QS-1

Following the reinforcement process, the cracking pattern was re-examined and depicted in Figure 35. Notably, no cracks were observed within the reinforced region, while cracking persisted in the surrounding areas. However, in certain analyses, cracks were identified even within the reinforced zone. This anomaly can be attributed to the heightened stress concentration in that specific region.

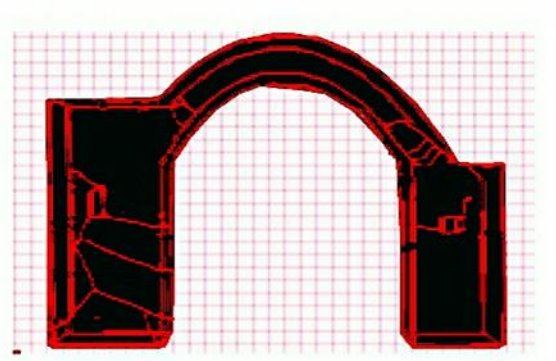

Fig. 35. Cracking pattern in QD-1

Figure 36 is a displacement/time diagram for the reinforced and unreinforced scenarios, showing that reinforcement improved structural strength and reduced displacement.

The base-shear/displacement diagram in Figure 37 also shows an improved performance after reinforcement.

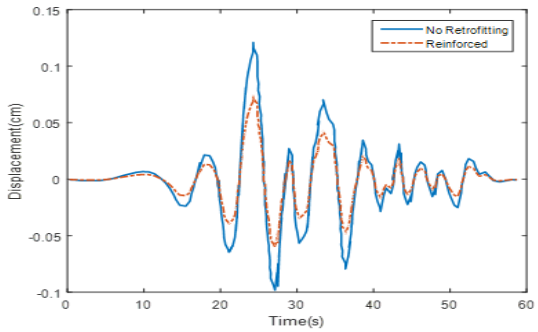

Fig. 36. Displacement/time diagram of QD-1

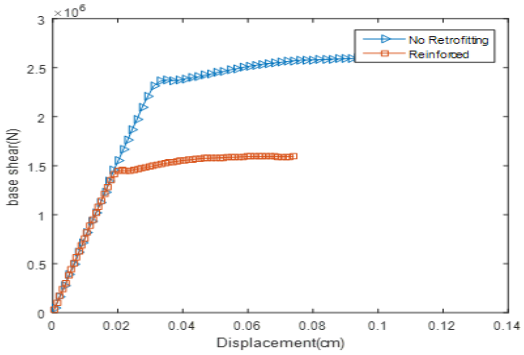

Fig. 37. Base-shear/Displacement diagram of QD-1

Figures 38 and 39 show, respectively, the place change/base shear hysteresis curve of QS-1 and QD-1 under the Sarpol-e Zahab earthquake. As expected, the curve is softer for the reinforced model.

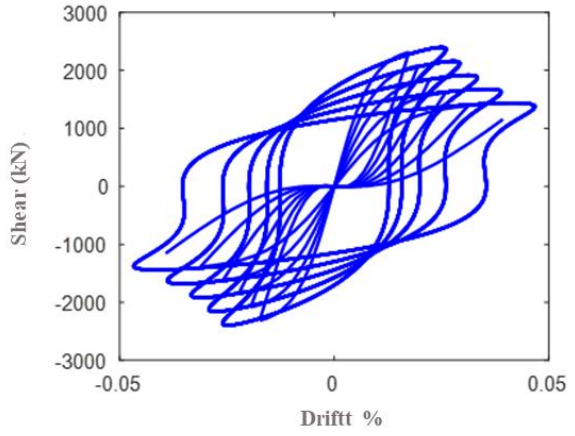

Fig. 38. Place change/base shear hysteresis curve of QS-1

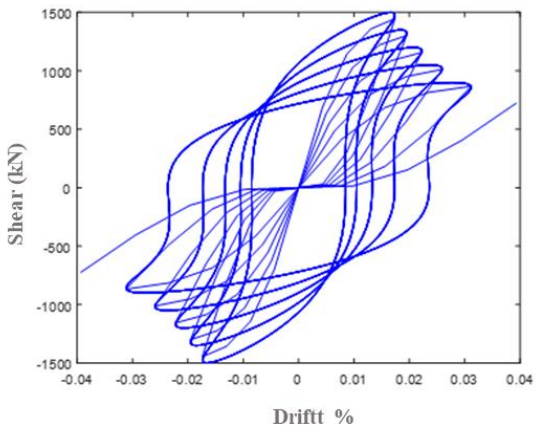

Fig. 39. Place change/base shear hysteresis curve of QD-1

As seen in the figures, energy absorption, ductility and behavior coefficient have increased by 16%, 47% and 43%, respectively, in the reinforced scenario compared to the unreinforced one. On the other hand, maximum Displacement and maximum shear have dropped by 63% and 64%, respectively. The findings from the strengthening of the first arch highlight significant enhancements in its structural behavior. Strengthening led to an approximately 16% increase in energy absorption compared to the unreinforced model, reflecting a notable improvement in its capacity to dissipate energy. Similarly, the ductility of the strengthened first arch showed a substantial enhancement, with an increase of nearly 47% compared to its normal counterpart, indicating greater deformation capacity under load. Moreover, the behavior factor of the strengthened first arch improved by approximately 43%, demonstrating enhanced structural performance under dynamic and seismic forces. In addition to these benefits, the maximum displacement of the strengthened arch decreased by around 63%, while its maximum base shear was reduced by approximately 64%, both compared to the unstrengthened condition. These results clearly illustrate the efficacy of the proposed strengthening technique in improving the structural robustness and performance of the first arch under various loading scenarios.

4.4. Results for the QS-2 arch model under the Sarpol-e Zahab earthquake

Figure 40 shows the cracking pattern in the second model under the Sarpol-e Zahab earthquake. The same pattern on the real arch is shown in Figure 41.

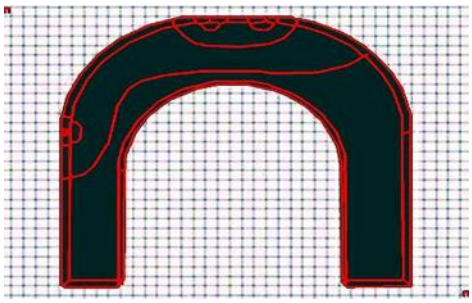

Fig. 40. Cracking pattern in QS-2

Fig. 41. Cracking pattern in QS-2

Figure 42 shows the cracking pattern in the second model under the Sarpol-e Zahab earthquake. Rebar placement and the applied mesh in this scenario are shown in Figures 43 and 44, respectively. The mesh is more concentrated in the reinforced area. Figure 45 shows the cracking pattern for the reinforced second model under the Sarpol-e Zahab earthquake. Compared to the unreinforced model, cracking has significantly decreased in this scenario. It should be noted that this reinforcement technique requires that the cracked area be determined before reinforcing the area with the NSM technique.

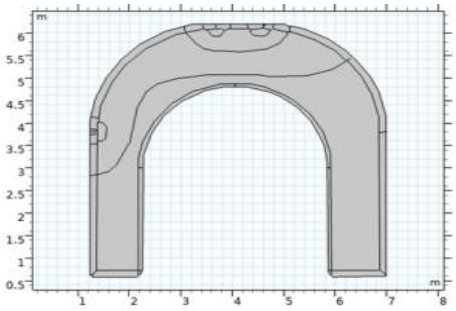

Fig. 42. Cracking pattern in QS-2

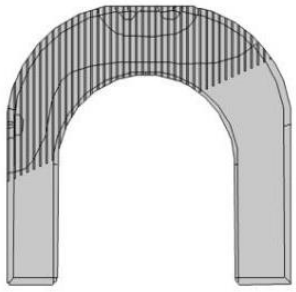

Fig. 43. Rebar placement in QS-2

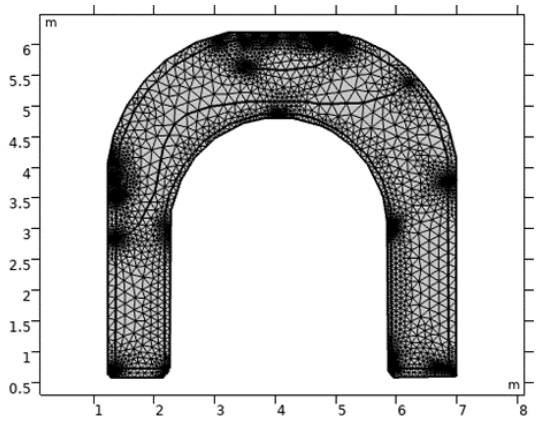

Fig. 44. Mesh applied after rebar placement in QS-2

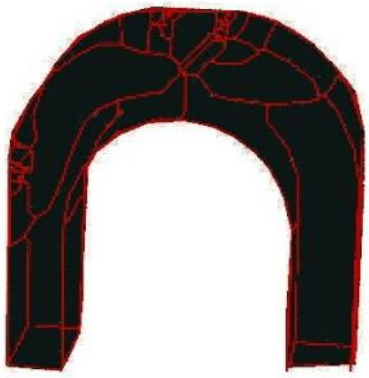

Fig. 45. Cracking pattern in QD-2 under the Sarpol-e Zahab earthquake

Figure 46 shows the time/displacement diagram for the second model under the Sarpol-e Zahab earthquake. The base-shear/displacement diagram is shown in Figure 47. Based on these diagrams, reinforcement adequately improves structural performance and increases structural strength by about 10%.

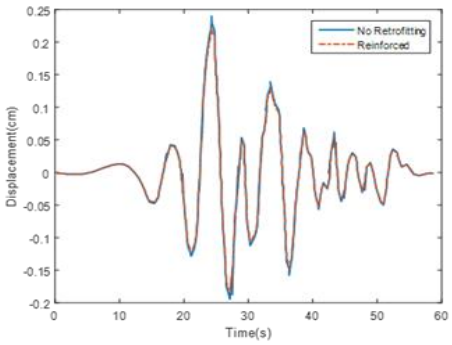

Fig. 46. Displacement/time diagram of the second model under the Sarpol-e Zahab earthquake

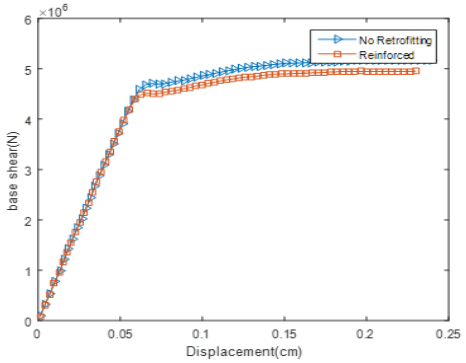

Fig. 47. Base-shear/displacement diagram of the second model under the Sarpol-e Zahab earthquake

Figures 48 and 49 show, respectively, the place change/base shear hysteresis curve of QS-2 and QD-2 under the Sarpol-e Zahab earthquake. As expected, the curve is softer in the reinforced scenario.

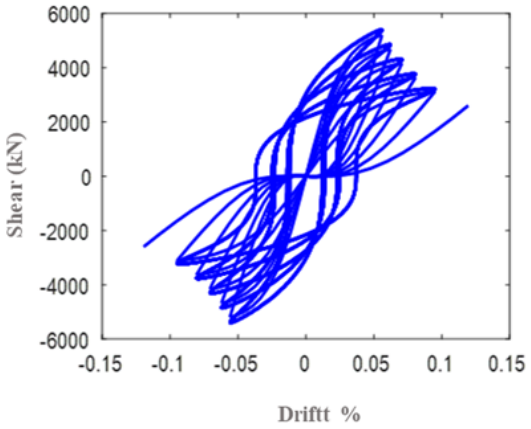

Fig. 48. Place change/base shear hysteresis curve of QS-2

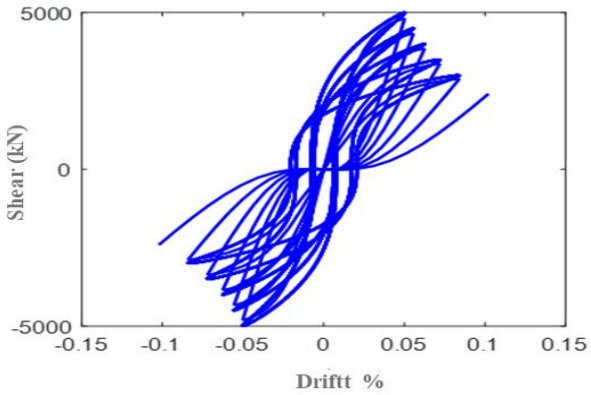

Fig. 49. Place change/base shear hysteresis curve of QD-2

Energy absorption, ductility and behavior coefficient have increased by 15%, 6.5% and 5.2%, respectively, in the reinforced scenario compared to the unreinforced one. On the other hand, maximum displacement and maximum shear have dropped by 7.1% and 7.3%, respectively. The strengthening of the QS-2 arch yielded significant enhancements in its structural performance. Specifically, energy absorption in the strengthened QS-2 model increased by approximately 15% compared to the unreinfirced configuration, reflecting an improved capacity for energy dissipation. In terms of ductility, the strengthened arch displayed a notable enhancement of about 6.5% over its unstrengthened counterpart, indicating greater flexibility and deformation capacity under loading. Moreover, the behavior factor of the QS-2 arch improved by approximately 5.2% as a result of the strengthening measures, highlighting a more robust structural response. The maximum displacement of the strengthened arch was reduced by roughly 1.7%, while the maximum base shear saw a decrease of approximately 3.7% in comparison to the unstrengthened state. These outcomes underscore the efficacy of the implemented strengthening approach in improving the structural stability and performance of the QS-2 arch.

4.5. Results for the QS-3 arch model under the Sarpol-e Zahab earthquake

Figures 50 and 51 illustrate the crack patterns of the third arch model without reinforcement, subjected to the Sarpol-e Zahab earthquake.

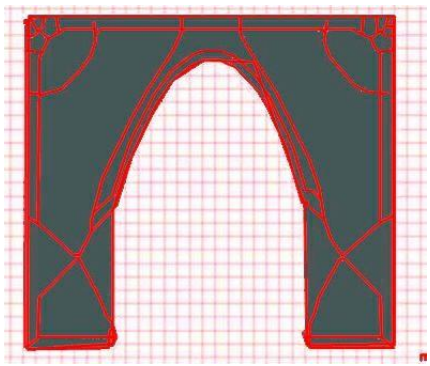

Fig. 50. Cracking pattern in QS-3

Fig. 51. Cracking pattern in QS-3

Figure 52 presents the crack pattern, while Figures 53 and 54 illustrate the reinforcementlayout and the type of mesh applied to the third arch model under the Sarpol-e Zahab earthquake.

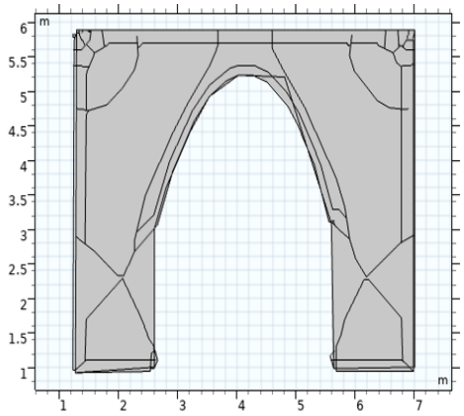

Fig. 52. Cracking pattern in QS-3

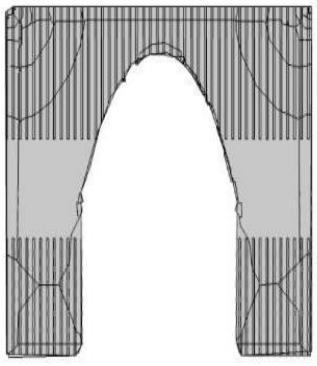

Fig. 53. Rebar placement in QS-3

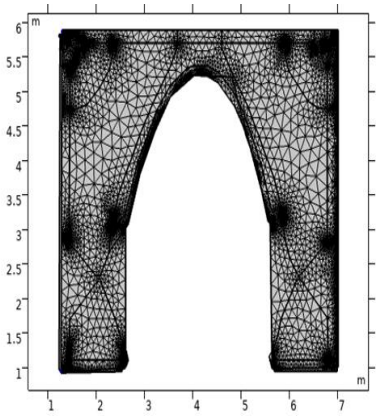

Fig. 54. Mesh applied after rebar placement in QS-3

Figure 55 depicts the crack pattern observed in the reinforced third arch model subjected to the Sarpol-e Zahab earthquake. When comparing this model to the unreinforced state, a noticeable 30% reduction in crack propagation is evident. While accurately quantifying crack growth reduction in a one-dimensional domain with numerous cracks presents challenges, the extent of this change can be effectively assessed through visual inspection and the discernible decrease in crack intensity.

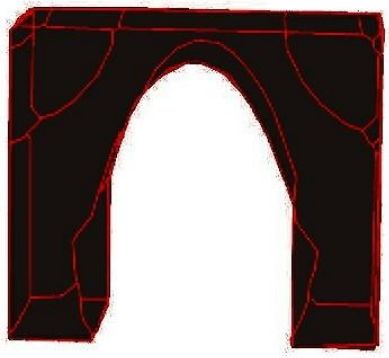

Fig. 55.Cracking pattern in QD-3 under the Sarpol-e Zahab earthquake

Figure 56 shows the displacement-time relationship for the third arch model under the Sarpol-e Zahab earthquake, highlighting a comparison between the reinforced and unreinforced conditions. Similarly, Figure 57 provides the base shear-displacement relationship for the same model during this seismic event.

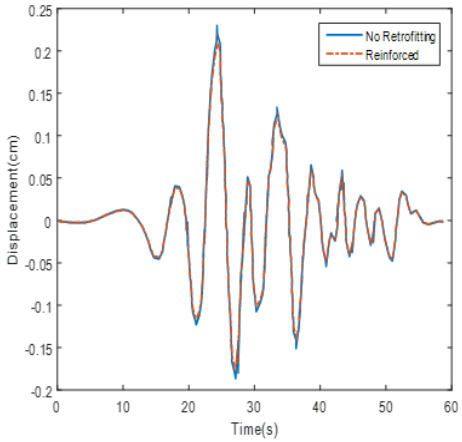

Fig. 56. Displacement/time diagram of the third model under the Sarpol-e Zahab earthquake

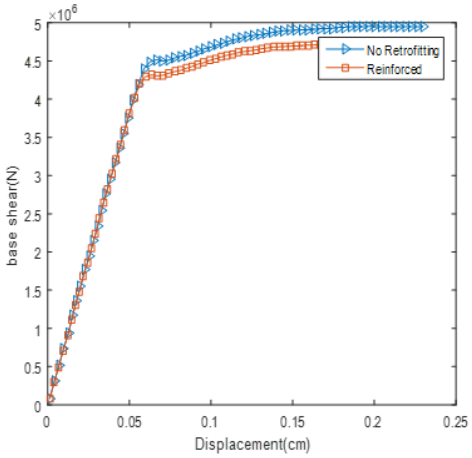

Fig. 57. Base-shear/displacement diagram of the third model under the Sarpol-e Zahab earthquake

Figure 58 depicts the hysteresis curve representing drift versus base shear for the unreinforced third arch model subjected to the Sarpol-e Zahab earthquake. In contrast, Figure 59 displays the corresponding curve for the reinforced model under the same seismic conditions. As anticipated, the reinforced model demonstrates a more consistent and organized hysteresis behavior.

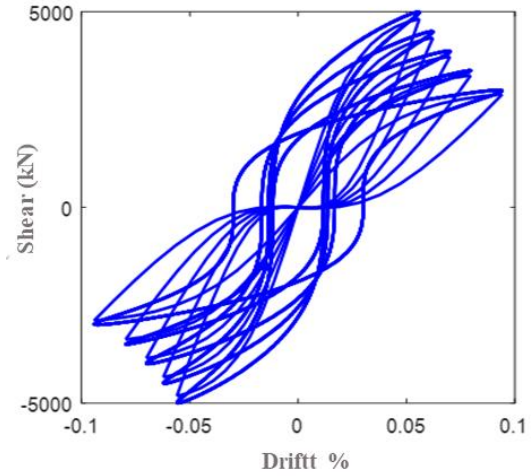

Fig. 58. Place change/base shear hysteresis curve of QS-3

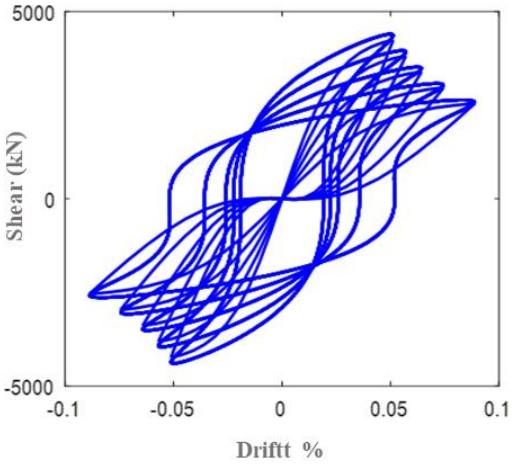

Fig. 59. Place change/base shear hys teresis curve of QD-3

The results of the QS-3 arch modeling, conducted using Abaqus finite element software, indicate notable enhancements in its structural performance following the implementation of strengthening measures. Energy absorption in the strengthened QS-3 arch increased by approximately 17% compared to its unstrengthen counterpart, signifying an improved ability to dissipate energy. Additionally, ductility in the QS-3 arch saw an approximate 7.7% increase after strengthening, reflecting enhanced deformation capacity under applied loads. The strengthening measures also resulted in an approximately 7.5% improvement in the behavior factor of the QS-3 arch, emphasizing better structural response and stability. Moreover, the maximum displacement of the QS-3 arch was reduced by roughly 14.5%, while the maximum base shear experienced a decrease of about 15.1% when compared to the strengthened state. These outcomes clearly demonstrate the effectiveness of the proposed strengthening strategy in improving the structural integrity and overall performance of the QS-3 arch.

4.5. Analysis of Crack Patterns

The findings from the modeling and crack propagation analysis of the studied samples demonstrated distinct patterns in different arches. In the QS-1 arch, the majority of cracks were concentrated at the interface between the arch roof and the adjoining walls or columns. For the QS-2 arch, cracks were predominantly located in the arch vault, specifically at the crown and haunch regions. Similarly, in the QS-3 arch, cracks were most commonly observed along the rise and in the columns. A comprehensive assessment of the arches further revealed that most of the detected cracks were transverse in orientation. Among these, the most critical and structurally compromising cracks occurred at the junction of the vault and columns, as well as near the base of the walls. The reinforcement approach proposed in this research has been shown to effectively mitigate the initiation and progression of such cracks, offering a promising solution to enhance the structural integrity of arches.

5. Conclusion

This research sought to bridge the existing gap by first creating a comprehensive model in ABAQUS to examine the general behavior of a representative arch. The most vulnerable section of the arch was subsequently identified and modeled as a sub-representative to reflect the structural response in greater detail. A simplified micro-level approach was employed, incorporating both frictional and cohesive interactions at the block-mortar interfaces. To assess the arch's dynamic performance, time-history analysis was conducted using acceleration data from major global earthquakes, as well as a notable event recorded in Iran. These seismic records were obtained from the Pacific Earthquake Engineering Research (PEER) Center's. The main takeaways from the analysis are as follows: (1) The findings from the modeling and analysis of the arches, both in unreinforced and reinforced conditions, reveal that the proposed reinforcement technique enhances the lateral resistance of arches by approximately 20%. Moreover, this method substantially improves the seismic performance and crack distribution patterns of the arches. Notably, this retrofitting strategy has minimal impact on the visual integrity and aesthetic appeal of the structure. (2) Among the analyzed models, the first arch displayed superior seismic resilience, as evidenced by parameters such as energy absorption, displacement capacity, ductility, behavior factor, and maximum base shear, when compared to the other two models. (3) A thorough investigation of the arches revealed that the majority of cracks were transverse in nature. However, the most critical and damaging cracks were located at the junction between the arch vault and the columns, as well as at the base of the columns. (4) The application of Near-Surface Mounted (NSM) reinforcement proved to be highly effective in mitigating the formation and propagation of these critical cracks, offering a significant improvement in structural performance and durability.

References

[1] Ahmadi, S., Meskin, H., & Rezalu, R. (2014). An analysis of Iranian arches with a special focus on five- and seven-centered arches. *Proceedings of the First Scientific Research Congress on New Horizons in Civil Engineering, Architecture, Culture, and Urban Management in Iran*, Tehran, Association for the Development and Promotion of Basic Sciences and Techniques.

[2] Shamsipoor Dehkordi, A., Jafari Farsani, M., & Naghdi Dorbati, Z. (2013). Stability of domes and arches with sustainable materials in traditional Iranian architecture. *Proceedings of the First National Conference on Geography, Urban Planning, and Sustainable Development*, Tehran, Komesh Environmental Association, University of Aviation Industry.

[3] Taifi Nasr-Abadi, A., & Rashidi Mehr-Abadi, M. H. (2008). Methods for retrofitting and strengthening adobe and masonry structures against earthquakes. *Journal of Civil Engineering, Islamic Azad University*, Special Issue 2, Fall 1387

[4] Frahad Akhoundi, Reza Mohammadpour, Yaser Shahbazi. Application of Near Surface Moumted (NSM) Technique Seismic Retrofitting of Heritage Building: Case Study of No.1 Educational Heritage Building of Tabriz Art University, Journal of Research on Archaeometry,2020; 6(1):97-118

[5] Pouraminian, M., & Sadeghi, A. (2010). Evaluation of the seismic behavior of Iranian circular arches and their analogues. *Proceedings of the First National Conference on Structures, Earthquake, and Geotechnics*, Babolsar, Iran.

[6] Karimi, A. H., & Eslami, A. (2017). Recognizing the structural behavior of conventional arches in traditional Iranian architecture. *Proceedings of the 11th International Congress on Civil Engineering*, University of Tehran, Tehran.

[7] Radahmadi, M. (2018). Static analysis of Iranian arches underweight load using the finite element method. *Proceedings of the 4th National Conference on Strengthening and Preservation of Permanent Buildings*, Arak.

[8] Button, M. R., Cronin, C. J., & Mayes, R. L. (2002). Effect of vertical motions on seismic response of bridges. *Journal of Structural Engineering*, *128*(12), 1551–1564.

[9] Pouraminian, M. (2022). Multi-hazard reliability assessment of historical brick minarets. *Journal of Building Pathology and Rehabilitation*, *7*(1), 10.

[10] Usta, P. (2021). Assessment of seismic behavior of historic masonry minarets in Antalya, Turkey. *Case Studies in Construction Materials*, *15*, e00665.

[11] Bahreini, V., Pouraminian, M., & Tabaroei, A. (2022). Seismic sensitivity analysis of Musa Palas historic masonry arch bridge by Tornado diagram. *Journal of Building Pathology and Rehabilitation*, *7*(1), 71.

[12] Cachim, P.B., 2009. "Mechanical properties of brick aggregate concrete". *Construction and Building Materials*, 23(3), pp. 1292-1297.

[13] Tighiouart, B., Benmokrane, B. and Mukhopadhyaya, P., 1999. "Bond strength of glass FRP rebar splices in beams under static loading". *Construction and Building Materials*, 13(7), pp. 383-392.

[14] Seyedsjadi, S. M. (2019). Natural environment and ancient monuments of Sistan plain. *Journal of Geographical Research*, (56–57), 146–186.

[15] Akbarzadeh Morshedi, A., & Taghi Panahi, F. (2020). Experimental investigation of the behavior of brick masonry arches (vault and rib cover) unreinforced and reinforced with C-FRP under simultaneous vertical and horizontal loads. *Advanced Research in Civil Engineering*, *2*(3), 41–50.

[16] Sakbana, A., & Mashreib, M. (2020). Finite Element Analysis of CFRP Reinforced Concrete Beams. *Journal of Construction Engineering*, 35, 148–169.